DTU Library

The role of substrate electrons in the wetting of a metal surface

Schiros, T.; Takahashi, O.; Andersson, Klas Jerker; Ostrom, H.; Pettersson, L.G.M.; Nilsson, A.; Ogasawara, H.

The role of substrate electrons in the wetting of a metal surface

T. Schiros,[1,2,a)] O. Takahashi,[2,3] K. J. Andersson,[4] H. Öström,[2] L. G. M. Pettersson,[2] A. Nilsson,[1,2,5,b)] and H. Ogasawara[1,2,5]

[1]*Stanford Synchrotron Radiation Lightsource, 2575 Sand Hill Road, Menlo Park, California 94025, USA*
[2]*FYSIKUM, Stockholm University, AlbaNova University Center, S-10691 Stockholm, Sweden*
[3]*Department of Chemistry, Graduate School of Science, Hiroshima University,*
Kagamiyama, Higashi-Hiroshima 739-8526, Japan
[4]*Department of Physics, Center for Individual Nanoparticle Functionality (CINF),*
Technical University of Denmark, Fysikvej 312, DK-2800 Kgs. Lyngby, Denmark
[5]*Stanford Institute of Materials and Energy Sciences, SLAC National Accelerator Laboratory,*
Menlo Park, California 94025, USA

We address how the electronic and geometric structures of metal surfaces determine water-metal bonding by affecting the balance between Pauli repulsion and electrostatic attraction. We show how the rigid d-electrons and the softer s-electrons utilize different mechanisms for the redistribution of charge that enables surface wetting. On open d-shell Pt(111), the ligand field of water alters the distribution of metal d-electrons to reduce the repulsion. The closed-shell Cu d^{10} configuration of isostructural Cu(111), however, does not afford this mechanism, resulting in a hydrophobic surface and three-dimensional ice cluster formation. On the geometrically corrugated Cu(110) surface, however, charge depletion involving the mobile sp-electrons at atomic rows reduces the exchange repulsion sufficiently such that formation of a two-dimensional wetting layer is still favored in spite of the d^{10} electronic configuration. © 2010 American Institute of Physics. [doi:10.1063/1.3292681]

I. INTRODUCTION

Knowledge of the contact layer of water on surfaces is of major importance for a number of processes such as heterogeneous and electrochemical catalysis, environmental corrosion, and weathering. Although the structure of the first water layers in contact with metal surfaces has been studied intensely,[1–17] we still lack an understanding of the fundamental interactions that govern the association of the first water layer to different surfaces. It is essential that we obtain a complete picture that elucidates the influence of both the d- and sp-electrons as well as the surface structure of the metal so we can predict trends in water-substrate bonding. A fundamental understanding of these trends is central to rational (electro)catalyst design, e.g., the fuel cell reaction, which is becoming increasingly important for its potential role in a clean energy economy. Obtaining a detailed picture of the metal-water interaction has been particularly difficult since the water molecule has a closed-shell electronic structure and thereby bonds only weakly to the surface and to other water molecules.

The particular issue of the thermodynamic stability of molecular wetting layers versus bulk ice I_h was addressed through density functional theory (DFT) calculations by Feibelman in his seminal science paper.[16] In that paper, he advocated that for a molecular wetting structure to exist, it needs to be more stable than bulk ice I_h (DFT-derived sublimation energy of $\Delta E_0 \sim 0.67$ eV/H_2O). Although a recently suggested molecular wetting structure on Ru(0001) comes close,[18] in almost eight years since Feibelman's publication, none of the many models proposed for molecular wetting structures on metal surfaces fulfill the thermodynamic criterion despite the use of state-of-the-art DFT calculations.

We do not propose a solution to this conundrum, which may have its roots in the insufficiencies (to a certain degree) in most DFT calculations, related to, e.g., the description of van der Waals forces, H-bonding interactions, quantum tunneling effects, zero-point vibrational energy, and issues around reliability of the employed functionals when dealing with different geometries, especially when comparing the different aggregation states of water, bulk ice I_h versus surface adsorbed water. Other effects may render bulk ice I_h to not be the appropriate reference state, such as the typically hydrophobic nature of the (H-down) molecular wetting layer toward water multilayers.[19–23] Furthermore, kinetic effects, which include, e.g., a possibly faster (or equally fast) incorporation of water into the two-dimensional (2D) wetting structure from three-dimensional (3D) ice clusters compared to monolayer desorption, also cannot be excluded.

For these many reasons, we choose in the present combined experimental and theoretical study not to focus on the exact DFT energetics but instead develop a chemical bonding picture, in which we demonstrate how the interplay between the repulsive interaction between the oxygen ($1b_1$) lone pair (lp) and the metal d-shell and attractive electrostatic interactions of the lp with the positive metal core determines the wettability of metal surfaces.

There are two main bonding mechanisms of water to metal surfaces (H-down bonding and O-bonding).[3] Here, we study in detail the O-bonding channel, which is responsible

a)Present address: Columbia University Energy Frontier Research Center (EFRC), 530 W. 120th St., Schapiro CEPSR, New York, NY 10027.
b)Author to whom correspondence should be addressed. Electronic addresses: nilsson@slac.stanford.edu and nilsson@ssrl.slac.stanford.edu.

for the dominant part of the metal-water bonding strength,[11] and use Pt(111), Cu(111), and Cu(110) surfaces as model systems to vary the population of the *d*-shell from open (Pt) to closed (Cu) and the surface geometric structure from flat (111) to corrugated (110). We focus on the chemical bonding of water at atop sites, although in the large unit cells of the experimentally observed wetting structures on Pt(111) and Cu(110) [$(\sqrt{37} \times \sqrt{37})R25°$ or $(\sqrt{39} \times \sqrt{39})R16°$ on Pt(111) (Refs. [24] and [25]) and (7×8) on Cu(110) (Ref. [26])], the exact water configurations (local structures) are unknown to date. Experimental and theoretical results, however, clearly show that monomer adsorption at metal surfaces occurs at atop sites,[17] and this site is also favored for other wetting structures on, e.g., Ru(0001) (Ref. [18]) and a low-coverage phase on Cu(110).[27] The preference for atop adsorption sites on Cu(110) and Pt(111) [and Ru(0001)] persists in *ab initio* molecular dynamics simulations of the molecular wetting layers even at room temperature conditions.[28,29] Our choice of molecular wetting structures for studying the water-metal chemical bond are based on the above obtained structural preferences and also the simpler periodicities of water monolayer wetting structures on Pt(111) $((\sqrt{3} \times \sqrt{3})R30°)$ and Cu(110) $(c(2 \times 2))$, induced by minute amounts of hydroxyl groups as dopants.[26,30]

Comparison to experimental x-ray absorption spectroscopy (XAS) data shows that the crucial electronic structure feature we discuss, the depopulation (or not) of the water O-bonding oxygen lp as a result of interaction with the conduction band and *d*-electrons, is captured very well by the (simplified) models we use with a more strongly bound atop O-bonding water anchoring to the substrate (and its next neighbor waters).[3,26] These computational models will be described in detail in Sec. II. To help disentangle the roles of the substrate *s*- and *d*-electrons and geometric versus electronic structure effects in water-metal bonding, we furthermore compare surfaces with empty *d*-bands, fcc Li(111) and Li(110), to the water-Cu systems.

II. METHODS

The experiments were performed at the undulator beamline I511 at the MAX laboratory and beamline 11.0.2 at the Advanced Light Source.[3,26] D_2O was utilized in order to minimize irradiation-induced dissociation.[31] X-ray photoelectron spectroscopy (XPS) and XAS spectra were obtained using total energy resolution better than 0.3 and 0.1 eV, respectively, using experimental conditions described in previous reports.[3,26,32,33] Monolayer water is defined to be the saturation coverage of the ideal monolayer[3,26] corresponding to 1×10^{15} water molecules/cm^2 on Pt(111) (Ref. [3]) and 1.1×10^{15} water molecules/cm^2 on Cu(110).[26] The water coverage was estimated from XPS using O 1*s* XPS calibration intensities for well-defined layers of CO with known saturation coverage as well as the XPS binding energy (BE) shift between the multilayer and the monolayer water. The monolayer of water was obtained by desorbing away water multilayers at 140 K; the absence of a multilayer XPS peak was confirmed. For water on Cu(111), the same molecular density as on Cu(110) was used to define the monolayer coverage, although on this hydrophobic surface no wetting monolayer forms.

The STOBE-DEMON program[34] was used for the theoretical analysis,[3,26,33,35] to perform constrained space orbital variation (CSOV)[36,37] analyses, and to compute charge density differences (CDDs) and XAS spectra for cluster models generated from periodic structures[3,26] optimized using the plane-wave based DACAPO program.[38] Clusters were kept as large as possible to ensure stability in the analysis of the energetics and to avoid artifacts in the computed spectra; the calculations were repeated for a range of cluster model sizes to determine the minimal number of atoms needed to avoid cluster size dependent artifacts and to ensure stable results. The trends in CSOV values presented are stable with respect to variation in the cluster size even for cluster models represented by as few as 10 atoms. This investigation allowed us to identify cluster models of the optimal size for stable results and computational efficiency so that any energetic variation with further increase in the cluster size was negligible for all surfaces. For instance, CSOV values for the center O-bonded water molecule in an H-down layer on Cu(111) were nearly identical for three-layer clusters of 37 Cu atoms (used here) and 59 Cu atoms; frozen orbital (FO) values were +0.39 and +0.42 eV, respectively, for the 37 and 59 Cu atom clusters, and interaction energies in the final relaxed step were −1.18 eV (37 Cu atoms) and −1.14 eV (59 Cu). A similar saturation of CSOV energy variation with cluster size was observed for Cu(110) clusters of 38 and 60 Cu atoms; the larger cluster was used to more directly connect with the previously published work.[26] This ensures that the FO values for the 37 atom Cu(111) cluster and the 60 atom Cu(110) cluster can be directly compared.

Following this investigation, the (111) surfaces were thus modeled with 37 metal atoms in three layers with 19 atoms in the first layer, 12 in the second, and 6 in the third as described in Ref. [33] for Pt, while 60 Cu atoms arranged in 4 layers, with 14 atoms in the first and third layers and 16 atoms in the second and fourth layers, represented the geometrically corrugated Cu(110) surface. Four water molecules, a center O-bonded water fully coordinated by three H-down molecules, provided a sufficient representation of the water monolayers on the metal clusters. Cartesian coordinates of the structures are provided as supplementary material.[39]

The CSOV energy decomposition scheme uses as reference the self-consistent energy and orbitals of the system where the central water has been moved to "infinite" (>50 Å) distance while keeping all other geometrical parameters fixed. The initial repulsion is then estimated by bringing the central water back without allowing any variational orbital relaxations (Frozen Orbital, FO, step); the orbitals are, however, orthogonalized and the system is always treated as a supermolecule. Although the CSOV energy decomposition scheme is based on a constrained minimization, this should not be confused with the constraints used in the subsystem embedding approach developed by Wesolowski and Warshel.[40] The constrained search in their approach to embedding is based on the Levy constrained search[41] defini-

tion of the kinetic energy, T_s, in which the orbitals are optimized under the constraint to yield a specific density. The CSOV procedure, on the other hand, is not an embedding technique but simply a decomposition of the interaction energy based on a controlled way to stepwise arrive at the final diagonal Kohn–Sham matrix.

In the present work we limit ourselves to the first, FO step in this procedure. This is performed by transforming the Kohn–Sham matrix to molecular orbital basis using orbitals for the cluster and adsorbate defined at large separation and thus well-defined apart from small contributions due to the orthogonalization. In the FO step all off-diagonal matrix elements coupling cluster and adsorbate orbitals, occupied as well as unoccupied, are set to zero, ensuring that no mixing or relaxation of orbitals can occur; this gives the initial interaction between the unrelaxed but orthogonalized wave functions. In the full CSOV procedure the number of off-diagonal elements, corresponding to specific orbital and physical interactions, included in the diagonalization is stepwise increased until all interactions are included and the full matrix is diagonalized, always, however, working with fully orthonormal orbitals and the full density based on these orbitals.

Finally, we also confirmed that possible differences in dipole interaction at the different surfaces due to choice of surface representation do not affect our CSOV energy values for the FO step. To test this, we eliminated this interaction by using a water molecule, artificially made linear to remove its dipole moment, as a surface probe and repeated the FO step at the same oxygen-metal distance with the molecule instead in this internal geometry; the main contribution to the FO energy is from the lp which is similar for the normal and linear geometry.

Comparing the FO adsorption energy (energy difference between the monomer at infinite separation from the surface and in its nominal position with all orbitals frozen from the separated system) for a normal and linear probe water at the Cu(111) and Cu(110) surfaces, we find insignificant differences in FO values. To ensure that this is not due to a fortuitous compensation by a quadrupole interaction, we confirmed that this is also true for different orientations of the linear molecule at the surface, and as function of the cluster size (for surfaces represented by 37 or more atoms and three or more layers as used here), which verifies that our FO values are not influenced by a varying dipole or quadrupole interaction energy at the different surfaces but directly reflect trends in the balance of attractive and repulsive components of the water-metal interaction. As an observation we note that a multipole expansion of the charge distribution of an extended cluster, valid at long range, is not, in general, a good representative of the resulting electrostatic interaction between a highly polarizable metal surface and a strongly bound adsorbate.

As discussed in the Introduction (Sec. I), c(2×2) and ($\sqrt{3} \times \sqrt{3}$) unit cells were used in the periodic boundary condition geometry optimizations for Cu(110) (Ref. 26) and Pt(111),[33] respectively, as in previous reports, which also give a description of the basis sets used in the cluster calculations.[3,26,33]

Consistent with nonwetting behavior, the optimized (H-down) structure for water on Cu(111) deviates from the wetting structures on Cu(110) and Pt(111) not only in a large O–Cu distance (3.36 Å) for the O-bonded water molecules but also in the O–O buckling (vertical displacement between O atoms). To facilitate direct comparison in the cluster calculations, the water layer on Cu(111) was calculated for the optimal O–Cu distance of 2.44 Å obtained for Cu(110).[26] Moreover, geometry optimization of an H-down monolayer on Cu(111) leads to the O-bonded waters sitting 0.13 Å farther from the surface than their H-down neighbors, as opposed to the hydrophilic Pt(111) and Cu(110) surfaces where the O-bonded molecules sit ~0.4 Å closer to the surface than their H-down counterparts. To avoid the unphysical situation of very short metal-H-down water (M-H_2O) bonds at the shorter O–Cu distance (2.44 Å), the O–O buckling in the Cu(111) cluster model was adjusted to mimic that of the hydrophilic Pt and Cu(110) surfaces using the geometry of the water layer on Pt(111) (Ref. 3) scaled by the Cu:Pt lattice constant ratio. We compared the CDD plots as a function of water-metal (H_2O-M) distance and found negligible effects for a small change of 0.1 Å, i.e. the difference between H_2O–Pt and H_2O–Cu bond lengths.

fcc Li [(111) and (110)] surfaces were also generated in order to isolate the roles of d- and s-electrons by a comparison of surfaces with empty (Li) and filled (Cu) d-bands, respectively. Specifically, we studied the interaction of a water monomer at Li(111) and Li(110) surfaces, with the structure obtained by scaling the corresponding H-down monolayer cluster models used for the Cu surfaces by the ratio of the fcc Li:Cu lattice constants; this resulted in an O–Li distance of 2.8 Å. This approach was based on the near-linear relationship between H_2O-M (monomer and H-down monolayer) and M-M nearest-neighbor distance extracted from an earlier DFT study on a range of transition metal surfaces.[42] However, a much shorter O–Li bond of 2.01 Å was obtained when the geometry of the H_2O monomer was actually optimized in the presence of the (fixed) Li(111) cluster, consisting of 37 atoms in three layers like the other (111) clusters. The large difference in the O–Li distance between the scaled Li structure, which used the atomic radii/fcc lattice parameters, and the optimized structure is mostly due to the significantly larger difference between atomic and ionic radii for Li compared to Cu; we will return to this in Sec. III. By reporting results for both situations, 2.8 and 2.01 Å, we cover situations (H_2O-M distances) expected on transition metal surfaces as well as on Li.

The metal atoms were described at the all-electron level using the DZVP2 DFT optimized basis set of Ref. 43 for the first layer of Cu(111) and the first two layers of the Cu(110) cluster, while a one-electron effective core potential (ECP) (Ref. 44) provided a sufficient description of the layers further from the surface. A 16-electron relativistic ECP developed by Wahlgren,[45] including also the $5s^2$ electrons in the ECP operator, was used to describe the Pt atoms; the form of the ECP follows that of Bonifacic and Huzinaga[46] and the size of the core represents a compromise between a large (including $5s$ and $5p$) and small ($5s$ and $5p$ as valence) core, avoiding difficulties with the large $5d$-$5p$ exchange interac-

tions. Although for $3d$ metals the $3d$-$3p$ and $3d$-$3s$ exchange interactions are of similar magnitude,[47,48] $5s$ can be expected to make a smaller contribution than each of the three $5p$ orbitals due to relativity. Parameters and orbital basis set for the Pt ECP are given in the supplementary material.[39] For the ground state of Pt_2, we find $r_e = 2.442$ Å and $D_e = 3.10$ eV compared to experimental $r_0 = 2.33297$ Å and $D_e = 3.14 \pm 0.02$ eV.[49] Similarly, for the difficult $^2\Delta$ state of PtH, we find $r_e = 1.607$ Å and $D_e = 2.69$ eV compared to experimental values of 1.528 Å and ≤ 3.44 eV;[50] the computed values for both PtH and Pt_2 are well within the range of other calculations—see discussions in Ref. 49 (Pt_2) and Ref. 51 (PtH). In the XAS calculations, the (core-excited) oxygen of the central water molecule in the cluster models was described using the IGLO-III all-electron basis set of Kutzelnigg *et al.*;[52] all other oxygen atoms were described using an ECP (Ref. 53) as in previous reports;[26,33] this eliminates their O $1s$ level and leads to the O $1s$ level of the target molecule being unique and nondegenerate ensuring in a very simple way convergence to the desired core hole state. The Li atoms were described using a double-zeta plus polarization basis set. Hydrogen and oxygen were described by triple-z plus polarization basis sets where the basis set for hydrogen has the $(5s)$ basis of Huzinaga[54] contracted to $3s$ and with one p-function added. We note that in the STOBE-DEMON calculations an auxiliary Gaussian basis set is used to expand the Coulomb potential and also that, during the iterations to reach self-consistency, an additional auxiliary basis is used to represent the exchange-correlation potential over the numerical grid to allow the use of a coarser grid to speed up the iterations; at convergence, the grid is tightened and the exchange-correlation contribution obtained by numerical integration without the auxiliary basis. Using the nomenclature $[(N_C(s), N_C(spd); N_{XC}(s), N_{XC}(spd)]$ to indicate the number of s (inner part) and spd-type (valence region, using the same exponents for s, p, and d) Gaussian functions used to fit and expand the Coulomb and exchange-correlation potentials, respectively, the auxiliary basis sets used were O $(5,2;5,2)$, H $(3,1;3,1)$, Cu $(5,5;5,5)$, and Pt $(5,5;5,5)$. Gradient-corrected exchange[55] and correlation[56] functionals were used throughout.

III. RESULTS AND DISCUSSION

First, we evaluate the hydrophilic and hydrophobic properties experimentally with O $1s$ XPS and XAS. The measurements shown here were conducted at 135 K, which is sufficient for water to overcome the activation barrier for the formation of thermally favored 3D islands on Cu(111)[6–8] and the uniform layer on Cu(110)[26,57] and Pt(111).[3] For water on Pt(111), the XPS peak at 532.2 eV [Fig. 1(a)] corresponds to water in direct contact with the Pt surface and indicates formation of a 2D water monolayer. The second water layer, characterized by a peak at 533 eV, begins to form only at coverage above 1 ML, as evidenced by a continuous shift in the peak position toward higher BE. In contrast, for water on Cu(111) [Fig. 1(b)] a very small chemical shift between sub-monolayer and multilayer coverages reveals that a 2D water layer does not form on the same surface plane of the noble
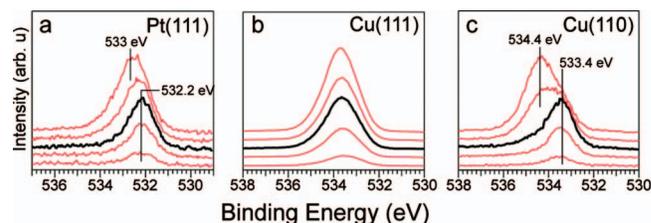

FIG. 1. O $1s$ XPS spectra measured during water uptake up to 2 ML coverage on (a) Pt(111), (b) Cu(111), and (c) Cu(110) at 135 K. The bold (black) spectra correspond to the monolayer coverage.

metal. This is in line with a recent scanning tunneling microscopy study of water on Cu(111) where 3D ice crystallites could be observed already at rather low coverage.[58] The XPS results in Fig. 1(c) show that the wetting behavior on Cu(110) is radically different from that on Cu(111) but rather similar to that on Pt(111). As for Pt(111), formation of a 2D water layer on Cu(110) is evidenced by a single low BE species (533.4 eV) for coverages up to 1 ML. Likewise, the shift in the peak position toward higher BE (534.4 eV) corresponds to multilayer growth, which for both Cu(110) and Pt(111) occurs only after completion of the first layer.

When the E-vector is parallel to the surface, XAS probes the electronic structure of the in-plane hydrogen-bond network, while the orthogonal polarization probes the water-metal bonds.[3,26,59] Free OH groups, i.e. water O–H neither hydrogen bonded to other water molecules[3,59] nor to the substrate,[3,26] produce a signature peak at 534.5–535 eV. For monolayer water on Pt(111), this peak is absent from both in-plane and out-of-plane XAS, which, along with the strong anisotropy between polarizations, confirms the formation of a uniform 2D hydrogen-bond network [see Fig. 2(d)].[3] In contrast, for the (111) surface of copper, the XAS spectrum [Fig. 2(b)] is completely isotropic; in- and out-of-plane spec-
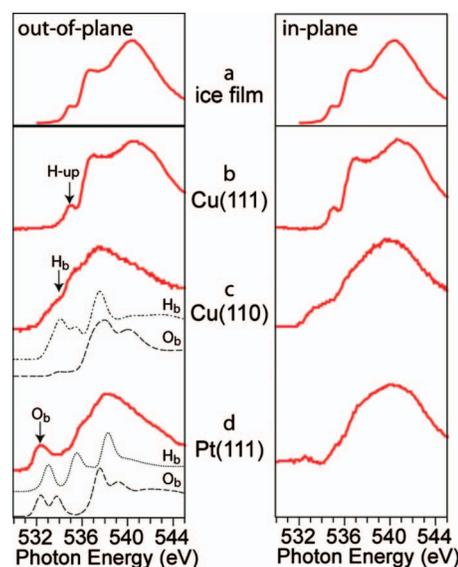

FIG. 2. O $1s$ XAS for monolayer water on (a) ice film (Ref. 60), (b) Cu(111), (c) Cu(110) (Ref. 26), and (d) Pt(111). The contribution to the signal from computed H-down bonding (H_b) and O-bonding (O_b) waters are indicated with dashed lines; characteristic resonances from different water species are indicated with arrows. The spectra were normalized to have equal maximum peak height.

tra are both nearly identical to the spectrum of the 3D bulk ice [Fig. 2(a)], indicating essentially no interaction with the metal. However, as seen in XPS, the interaction of water with Cu is very different when the (110) crystal plane is exposed. In the XAS spectra for Cu(110) [Fig. 2(c)], the polarization dependence confirms the well ordered 2D monolayer indicated by XPS. The larger intensity of the free OH peak at 535 eV for Cu(110) compared to Pt(111) shows that the reduced preference for H-down bonding on Cu results in a fraction of the OH groups pointing away from the (110) surface.[26]

Since the (111) surface structure is nearly identical for Cu and Pt, the difference in wetting ability must be attributed to the electronic structure; Cu represents a metal with nearly filled d-band, whereas Pt has a much larger fraction of d-holes. This indicates that, in agreement with the popular "d-band model,"[61,62] the degree of d-band population is important for the bonding of water to the metal surface. However, it is quite remarkable in the case of Cu that two different surface planes of the same metal can show such dramatically different bonding characteristics.

In order to explain these observations, we will paint a picture where the interaction of the water lp orbital ($1b_1$) with the metal gives rise to two counteracting forces: Pauli repulsion and electrostatic interaction via dative bonding. The localized d-electrons and the mobile sp-electrons respond rather differently to mitigate Pauli repulsion. It is usually energetically rather costly to radically change the d-population on a specific atom, and therefore rehybridization between different spatially oriented d-orbitals on the same atom is preferred as a means to remove charge from the direction of the repulsive overlap; this channel is, however, not open in the case of Cu. The sp-electrons, on the other hand, are much more mobile and can easily move away from the bonded metal atom toward neighboring atoms to minimize the overall repulsion. This mechanism leaves the metal atom positively charged so that charge can be donated from the water lp to the exposed metal ion core to form a coordination bond of highly polar character, i.e. a *dative bond*. For the H-down bilayer on Cu(110), Ren and Meng[63] estimated a net charge transfer of 0.17 electrons per unit cell to Cu. This may partly be ascribed to the dative bond formation, but likely less important than the large charge buildup between H and Cu for the H-down H_2O as the OH σ^* orbitals of H_2O accept charge in the H-down configuration.[3]

First, we demonstrate that it is possible to experimentally observe the lp-d-electron interaction from an analysis of the O 1s XAS spectra; since O 1s XAS measures the empty states with O 2p character, it becomes very sensitive to any loss of charge from the lp. Figure 2(a) shows a decomposition of the out-of-plane spectra into contributions from H-down bonding (M-HO) and O-bonding (M-O) waters. In the O-bonding channel, the interaction of the O lp ($1b_1$) orbital with the substrate d-band results in bonding and antibonding combinations[3] involving the oxygen lp and the metal d-bands–the "d-band model,"[61,62] as depicted in Fig. 3(a). In the case of water on Pt, the antibonding component of the O-bonding channel is not fully occupied. This indicates a mechanism for water to polarize charge to depopulate
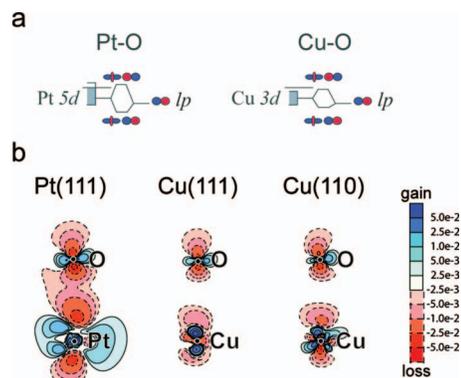

FIG. 3. (a) Schematic diagram of the Pt–O and Cu–O bonding interactions illustrating the larger splitting between bonding and antibonding states on Pt compared to Cu. The horizontal line perpendicular to the density of d-states indicates the Fermi level position, which falls below and above the antibonding states for water on Pt and Cu, respectively, and the different colors in the orbital plots represent different signs of the wave function. (b) CDD plots for metal-O bonding species for Pt(111) (Ref. 3), Cu(110), and Cu(111) (in electrons/Å^3).

the O lp to minimize Pauli repulsion and allow bonding. The depopulation is seen as a peak at 532.5 eV in the out-of-plane XAS spectrum, directly attributable to the O-bonding channel.

Conversely, the d-band of Cu is generated by the fully occupied 3d orbitals, which are more spatially contracted and less easily modified than the 5d orbitals of Pt(111). The contraction gives rise to a smaller splitting between the bonding and antibonding states on Cu(111) and Cu(110) compared to on Pt(111), as illustrated in Fig. 3(a). In the interaction with the closed-shell water lp both bonding and antibonding states become fully occupied, leading to Pauli repulsion. Accordingly, no such O-bonding related peak appears in the XAS for either Cu surface; the net charge transfer estimated on Cu(110) (Ref. 63) is not sufficient to give a measurable peak in XAS.

The degree of Pauli repulsion, excluding the sp-contribution, depends on the occupation and overlap of the O lp of water with the axial d-orbitals in the metal, which can be mitigated by charge redistribution. The computed charge rearrangements upon O-bonding for water on Pt and Cu are shown in Fig. 3(b) where the CDD is taken as the charge density of the fully relaxed system minus the sum of the charge densities of the cluster and overlayer computed separately. The CDD thus contains contributions both from the region of overlapping densities (Pauli exclusion) and from adsorption-induced charge rearrangements where the latter dominates as seen from the orbital-like character of the CDDs. The depopulation of charge from the O lp, indicated by the oxygen contribution to the unoccupied density of O–Pt antibonding states at 532.5 eV in the XAS, is clearly observed in the CDD plot [Fig. 3(b), left]. Pauli repulsion with the water lp orbital is further reduced by a redistribution of Pt d-electrons from axial d-orbitals to empty equatorial d-orbitals. This is seen in the respective decrease and increase in the occupation of axial and equatorial d-orbitals in the CDD plots (Mulliken population analysis becomes unreliable here due to the size of the clusters and the use of diffuse exponents in the Pt d-basis). We observe a similar

increase in charge density in the equatorial plane of the water molecule perpendicular to the oxygen lp. Since the CDD is taken between the combined system and separated overlayer and cluster, this result indicates a degree of cooperativity between surface and hydrogen bonding. We conclude that these two channels of charge rearrangement upon interaction with the *d*-electrons, i.e. a partial emptying of the O lp and loss of electrons in the axial *d*-orbital, allow the penetration of water lp into the charge cloud of the metal to establish the dative bond; note that this mechanism is different from the atomic *s* to *d* demotion discussed earlier by Harris and Andersson.[64]

In contrast, since both bonding and antibonding states are completely occupied for Cu, the mechanism of depopulation of the O lp is less available and the degree of charge redistribution of O-bonding water on Cu(111) and Cu(110), seen in Fig. 3(b), is much smaller than that observed for Pt(111). Although the ligand effect of water favors the occupation of equatorial *d*-orbitals over that of axial *d*-orbitals, the total occupation of these orbitals hardly changes because of the closed *d*-shell character of Cu.

The question emerges: With no unoccupied *d*-states available to facilitate depopulation of the O lp and reduce Pauli repulsion, what permits Cu(110) to be hydrophilic?

On Cu(110) an effective redistribution of charge is already satisfied through the Smoluchowski effect[65] of electron density smoothing at a corrugated surface, i.e. the itinerant *sp*-electrons preferentially occupy the space between, rather than atop, the atomic rows.[66] As a result, the electron density on the metal atom that coordinates to water is automatically reduced without repulsion-driven polarization; this not only reduces the repulsion but also opens for attractive electrostatic interactions,[36,67] allowing dative bonding between the O lp and the positive core of the bonded metal. We anticipate a similar attractive interaction on the (111) surfaces but with the additional energy cost to polarize the itinerant *sp*-electrons to achieve a slightly positive metal core.[36,67] The partially occupied *d*-states of Pt(111) serve to reduce the repulsion through internal charge rehybridization, whereas for Cu(110), the Smoluchowski effect allows an attractive electrostatic interaction via interatomic charge rearrangements of the mobile *sp*-electrons. Clearly, both the electronic and geometric structure effects influence the balance between attractive and repulsive interactions that dictates water-metal bonding.

We can isolate the connection between geometric structure and *s*-band polarization by using a Li metal surface to represent the idealized case of just a positive metal core and one valence *s*-electron per atom. fcc Li(110) and fcc Li(111) surfaces are employed to model the corrugated and flat surfaces. Since there is no orbital interaction with the Li 1*s* core orbital, we can isolate the interaction of the *s*-band with the water molecule. We can identify aspects of the charge rearrangement due to polarization and charge transfer for a water monomer on the corrugated and flat surfaces of Li by plotting how the charge has changed due to adsorption as shown in Fig. 4 at the two distances (2.8 and 2.0 Å). It will also provide insight into the role of the *s*-band in water-metal bonding not easily obtained from the CDD plots for Cu and
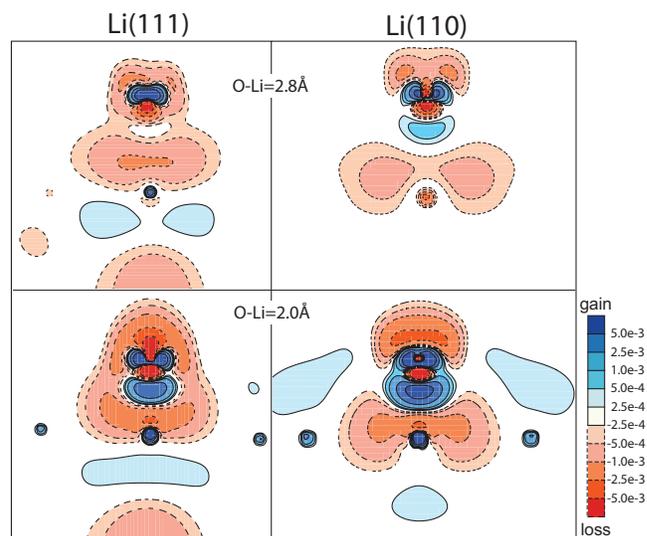

FIG. 4. CDD plots for O-bonded monomer on fcc Li(111) (left) and Li(110) (right) (cut along the [110] ridge) at 2.8 and 2.0 Å (electrons/Å^3).

Pt, which are dominated by rearrangements in the electron-rich *d*-shell, which has a much higher gradient in the charge density.

The CDD plots allow us to visualize how the O lp interacts with the *s*-electrons of the Li substrates (Fig. 4). Charge is removed from the metal atom coordinated to the water molecule by redistribution of metal *s*-electrons toward the neighboring atoms, which can be described in a simplistic way as the water lp "digging a hole" in the *s*-band, shown schematically in Fig. 5. Since there is now a partial positive charge on the metal atom, the lp orbital will be stabilized through electrostatic interaction, a mechanism often denoted as dative bonding; this is similar to water solvation of a cation in aqueous solution. The electrostatic dative bonding accounts for the main contribution to the bonding of water to metals and is illustrated in Fig. 4 by the accumulation of charge between the bonding units along the H_2O-Li axis as the O lp polarizes toward the Li atom. While the attractive component of the bonding is facilitated by the O lp digging a hole in the metal *s*-band, the (Pauli) repulsive contribution is minimized by a depopulation of O lp electrons along the water-metal axis, as indicated in Fig. 4 by the (red region, dashed line) vertical envelope of charge depletion, also observed for the Pt and Cu surfaces [Fig. 3(b)]. A noteworthy
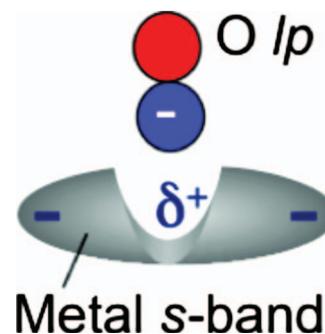

FIG. 5. Schematic illustration of the water O lp orbital "digging the hole" in the metal *s*-band to open for water-metal dative bonding as discussed in text.

difference between the Li and Cu systems, however, is that the optimal H_2O-M distance for Li does not scale with that for Cu as on transition metal surfaces (see also Sec. II),[42] which would lead to an H_2O–Li distance of 2.8 Å, but, in fact, is much shorter, only 2.01 Å. The much larger difference in atomic and ionic radii for Li compared to Cu allows a much closer approach of the water molecule to the metal surface without significant Pauli repulsion. This underlines not only how the orbital extent of the metal d-electrons really sets the limit on the H_2O-M bond length but also, and importantly, that the Li atom is becoming ionic in character as charge polarizes away from the Li atom coordinated to water and toward neighboring Li atoms at the surface. The Li $1s$ level contracts in response to the polarization of the Li $2s$ electron; this appears as a concentrated gain of charge on the Li atoms in Fig. 4. Finally, we note that although the degree of charge rearrangement increases with decreasing O–Li distance, as expected, the general features are the same.

There are, however, some revealing differences in the charge redistribution for the different Li surfaces. The reduced charge along the (110) rows makes the metal atoms already positive without any significant need for redistribution in order to open for dative bonding. Consequently, the gain of charge along the H_2O-metal axis indicative of dative bonding between the O lp electrons and the positive Li atom exposed by the "digging of the s-band hole" is larger for Li(110) than Li(111) at both distances. In this case we can directly observe the effect of the dative bonding in the polarization of the lp orbital toward the positive metal atoms. Furthermore, the slightly positive metal atoms of the (110) rows, charge depleted by the Smoluchowski effect, can more readily accept charge from neighboring metal atoms compared to those at the (111) surface; this is manifest in a gain of charge at the neighboring Li atoms (see Fig. 4, bottom right).

To gain deeper insight into the energetics of the geometric and electronic structure effects, we use CSOV analysis[36,37] to estimate the initial Pauli repulsion and relaxation energy of water on the different surfaces. The Coulomb contributions to dative bonding, i.e. the interaction between the oxygen p_z protruding lp orbital and metal ion core, cannot be separated from the exchange-driven Pauli repulsion in our implementation of the CSOV analysis since the orbitals are always orthogonalized; we note that alternative approaches do exist, e.g., Refs. 68 and 69, in which the electrostatic and exchange contributions are separated by computing the electrostatic contribution from the orbitals without antisymmetrization between the subsystems. In the present case, we can, however, circumvent any ambiguity introduced from using nonorthogonal orbitals by constructing the comparison to directly allow conclusions to be drawn on the relative importance of Pauli repulsion for (110) and (111) surfaces.

We thus compute the overlayer on the (111) surface at the same overlayer distance as for (110), which gives equivalent Coulomb contribution for the frozen lp interaction with the positive metal ion core, such that the difference in interaction energy between the two surfaces at this step is directly related to the Pauli repulsion; here, we will focus on this

difference. In the first step the central O-bonded water is well separated (50 Å) from the rest of the system in order to obtain separated orbitals and a reference energy value. Next the center water molecule is brought into contact with the rest of the system but with all molecular orbitals frozen (FO) as determined for the separated system, which brings out the initial interaction due to exchange and Coulomb interactions without any orbital relaxation; note that in this step the orbitals are orthogonalized but, apart from this, not allowed to mix in the variational procedure (see Sec. II). In the final step the system is fully relaxed and the overall BE in the adsorption process is obtained.

The CSOV analysis for water monomer on the two Li surfaces illuminates the balance between Pauli repulsion and electrostatic attraction that rules water-metal bonding. The reduced charge density on the (110) ridges and enhanced ability of the corrugated surfaces to redistribute charge reduces the energetic cost of polarization of the Li atoms (digging the s-band hole). Consequently, we observe a lower FO value for Li(110) compared to Li(111). In fact, the initial FO repulsion found for Li(111) (+0.06 and +0.29 eV at H_2O–Li distances of 2.8 and 2.0 Å, respectively) is eliminated on the Li(110) surface and instead replaced by attraction (−0.06 and −0.22 eV at H_2O–Li distances of 2.8 and 2.0 Å, respectively) due to the Smoluchowski effect.[65] The larger absolute values at the shorter distance are due to the greater overlap between O lp and Li s-electrons in the case of Li(111) and, alternatively, the enhanced electrostatic attraction between the O lp and the charge-depleted rows of Li(110). Here, we have a mechanistic explanation for the initial attraction (FO) which we find also for Cu(110) (discussed later) and expect to be valid for geometrically corrugated metal surfaces, steps,[13,42] and kinks, i.e. low-coordination sites, in general.

Let us take a closer look at the H-down water layers on Pt and Cu using the CSOV analysis. The water-metal systems are represented by a central O-bonded water surrounded by three water molecules adsorbed in the H-down geometry on metal clusters with three or four layers of atoms. Note that in this construct, with the central water being brought into bonding to the surface and to the three surrounding waters, the CSOV relaxation energy includes hydrogen bonding to the three neighboring waters and the BE to the metal, possibly modified by the three surrounding waters. As such these values cannot be directly compared to the BE for water monomers or overlayers on these surfaces. Furthermore, since the reference energy is defined for a system where the surrounding H_2O are kept in the same geometry with and without the central water, our energetics also contains the unrelieved strain in the initial configuration where the central molecule simply has been removed without structural relaxation of the surrounding waters. We also note that it has been shown that the H-bonding energetics is near constant from one metal to the next[12,70] so that trends in both FO and electronically fully relaxed interaction energy (E_{int}) from one metal surface to the next should mainly reflect changes in the water-metal component of the interaction.

Without reorganization of electronic structure (FO), we find that the initial repulsion is larger on Pt(111) than on isostructural Cu(111), 1.08 and 0.4 eV, respectively, due to

the larger extent of the more diffuse Pt 5*d*-orbitals. However, due to the greater ability to rehybridize these orbitals compared to the filled Cu 3*d* (Ref. 10) shell, the relaxation energy is also much greater for water on Pt(111) compared to Cu(111); 2.38 and 1.45 eV, respectively. The effect of geometric structure is highlighted when we compare the initial energetics for Cu(111) and isoelectronic Cu(110) in this analysis. As found for Li(110), due to the corrugation of charge at the Cu(110) surface, the initial interaction between water and the Cu in the FO configuration is actually attractive (−0.04 eV); i.e. the electrostatic attraction to the positive Cu core due to the charge redistribution of the delocalized *sp*-band caused by the Smoluchowski effect[65] more than compensates for the repulsive contribution from the more rigid *d*-band for Cu(110). We can envisage that the dative bonding in both cases proceeds via the O lp "digging an *s*-band hole" through polarization of charge away from the metal in a direction perpendicular to the water-metal bond to expose its positive metal core (see Fig. 5). On the geometrically corrugated Cu(110) surface, however, the exposed atomic rows are already partially depleted of charge which opens the surface for dative bonding with substantially lower energy cost for polarization.

Recently, a study of the nature of a single water molecule bonding to various 4*d* transition metal surfaces was conducted[71] using DFT. Also in that study a trend relating the position of the *d*-band to the water lp and metal *d*-electron interaction similar to the current study was found. Although the picture in Ref. 71 is more in terms of a covalent interaction by depopulation of the lp-*d* antibonding states, a connection was made to the picture, as discussed in the current study, that this interaction reduces the Pauli repulsion.[3] Both pictures become compatible with similar trends in terms of *d*-band center and population but the question is when the antibonding states have depopulated enough, upon moving toward the left in the periodic table, for the *d*-interaction to become attractive. Clearly, Ru will provide less repulsive or more attractive interaction to water than does Pd or Ag, but at which position the zero level in terms of attraction or repulsion is found is not given in that study. What was not included in Ref. 71 is the importance of the *sp*-electron polarization to open up for electrostatic interaction with the ionic core of the bonded metal atom. However, major rearrangements of the *sp*-electrons in the metal upon water coordination were identified in Ref. 71 supporting the *s*-band hole picture presented here.

IV. CONCLUSIONS

We conclude that the affinity of metal to water is ruled by the degree of Pauli repulsion between water lp and metal *d*- and *sp*-electrons and the attractive electrostatic interaction, which is determined by both the electronic and geometric structure of the substrate. There are three main channels to deplete charge along the water-metal bond axis which mitigate the repulsion and open for electrostatic dative bonding between the O lp and the resulting charged metal core: (i) a large spatial overlap between the lp and *d*-orbitals results in the formation of bonding and antibonding orbitals. Partial depopulation of the antibonding component through rehybridization polarizes water in a manner that significantly reduces the lp occupation. (ii) On open *d*-shell metals, the ligand field effect of water alters the stability of axial and equatorial *d*-orbitals, moving charge away from the water-metal bond axis. Closed *d*-shell metals, however, do not allow for this mechanism. A similar mechanism of moving charge is also observed between the axial O lp orbital and the equatorial internal OH bonding orbitals. (iii) The electron density smoothing effect on rough surfaces causes the mobile *sp*-electrons to occupy the space in between the atomic surface rows resulting in depletion of charge on the bonded metal atoms. This reduces the initial repulsion and also opens for a much stronger attractive electrostatic interaction through dative bonding, allowing bonding even in cases where internal *d*-shell rehybridization is unfavorable. Since the electron density smoothing effect is a general phenomenon at low-coordination sites, we predict reduced Pauli repulsion and increased electrostatic attraction for water at low-coordination sites (e.g., steps and kinks) on metal surfaces, in general.

[1] P. A. Thiel and T. E. Madey, Surf. Sci. Rep. **7**, 211 (1987).
[2] M. A. Henderson, Surf. Sci. Rep. **46**, 1 (2002).
[3] H. Ogasawara, B. Brena, D. Nordlund, M. Nyberg, A. Pelmenschikov, L. G. M. Pettersson, and A. Nilsson, Phys. Rev. Lett. **89**, 276102 (2002).
[4] B. D. Kay, K. R. Lykke, J. R. Creighton, and S. J. Ward, J. Chem. Phys. **91**, 5120 (1989).
[5] M. Klaua and T. E. Madey, Surf. Sci. **136**, L42 (1984).
[6] B. J. Hinch and L. H. Dubois, Chem. Phys. Lett. **181**, 10 (1991).
[7] B. J. Hinch and L. H. Dubois, J. Chem. Phys. **96**, 3262 (1992).
[8] J. Stähler, M. Mehlhorn, U. Bovensiepen, M. Meyer, D. O. Kusnierek, K. Morgenstern, and M. Wolf, Phys. Rev. Lett. **98**, 206105 (2007).
[9] S. Meng, E. G. Wang, and S. Gao, J. Chem. Phys. **119**, 7617 (2003).
[10] S. M. Dounce, S.-H. Jen, M. Yang, and H.-L. Dai, J. Chem. Phys. **122**, 204703 (2005).
[11] A. Michaelides, V. A. Ranea, P. L. de Andres, and D. A. King, Phys. Rev. Lett. **90**, 216102 (2003).
[12] A. Michaelides, Appl. Phys. A: Mater. Sci. Process. **85**, 415 (2006).
[13] M. Morgenstern, T. Michely, and G. Comsa, Phys. Rev. Lett. **77**, 703 (1996).
[14] A. Verdaguer, G. M. Sacha, H. Bluhm, and M. Salmerón, Chem. Rev. (Washington, D.C.) **106**, 1478 (2006).
[15] A. Michaelides and K. Morgenstern, Nature Mater. **6**, 597 (2007).
[16] P. J. Feibelman, Science **295**, 99 (2002).
[17] A. Hodgson and S. Haq, Surf. Sci. Rep. **64**, 381 (2009).
[18] S. Haq, C. Clay, G. R. Darling, G. Zimbitas, and A. Hodgson, Phys. Rev. B **73**, 115414 (2006).
[19] G. A. Kimmel, N. G. Petrik, Z. Dohnálek, and B. D. Kay, Phys. Rev. Lett. **95**, 166102 (2005).
[20] G. A. Kimmel, N. G. Petrik, Z. Dohnálek, and B. D. Kay, J. Chem. Phys. **126**, 114702 (2007).
[21] S. Haq and A. Hodgson, J. Phys. Chem. C **111**, 5946 (2007).

[22] I. Waluyo, D. Nordlund, L.-Å. Näslund, H. Ogasawara, L. G. M. Pettersson, and A. Nilsson, Surf. Sci. **602**, 2004 (2008).

[23] G. Zimbitas, S. Haq, and A. Hodgson, J. Chem. Phys. **123**, 174701 (2005).

[24] A. Glebov, A. P. Graham, A. Menzel, and J. P. Toennies, J. Chem. Phys. **106**, 9382 (1997).

[25] J. Harnett, S. Haq, and A. Hodgson, Surf. Sci. **528**, 15 (2003).

[26] T. Schiros, S. Haq, H. Ogasawara, O. Takahashi, H. Öström, K. Andersson, L. G. M. Pettersson, A. Hodgson, and A. Nilsson, Chem. Phys. Lett. **429**, 415 (2006).

[27] J. Carrasco, A. Michaelides, M. Forster, S. Haq, R. Raval, and A. Hodgson, Nature Mater. **8**, 427 (2009).

[28] S. Izvekov, A. Mazzolo, K. VanOpdorp, and G. A. Voth, J. Chem. Phys. **114**, 3248 (2001).

[29] S. Schnur and A. Gross, New J. Phys. **11**, 125003 (2009).

[30] C. Clay, S. Haq, and A. Hodgson, Phys. Rev. Lett. **92**, 046102 (2004).

[31] K. Andersson, A. Nikitin, L. G. M. Pettersson, A. Nilsson, and H. Ogasawara, Phys. Rev. Lett. **93**, 196101 (2004).

[32] K. Andersson, A. Gomez, C. Glover, D. Nordlund, H. Öström, T. Schiros, O. Takahashi, H. Ogasawara, L. G. M. Pettersson, and A. Nilsson, Surf. Sci. **585**, L183 (2005).

[33] T. Schiros, L.-Å. Näslund, K. Andersson, J. Gyllenpalm, G. S. Karlberg, M. Odelius, H. Ogasawara, L. G. M. Pettersson, and A. Nilsson, J. Phys. Chem. C **111**, 15003 (2007).

[34] K. Hermann, L. G. M. Pettersson, M. E. Casida, C. Daul, A. Goursot, A. Koester, E. Proynov, A. St-Amant, D. R. Salahub, V. Carravetta, A. Duarte, N. Godbout, J. Guan, C. Jamorski, M. Leboeuf, M. Leetmaa, M. Nyberg, L. Pedocchi, F. Sim, L. Triguero, and A. Vela, STOBE-DEMON; STOBE-DEMON version 5.3, DEMON Software, Stockholm, Berlin, 2005. The program can be obtained from http://w3.rzberlin.mpg.de/~hermann/StoBe/index.html.

[35] L. Triguero, L. G. M. Pettersson, and H. Ågren, Phys. Rev. B **58**, 8097 (1998).

[36] P. S. Bagus, K. Hermann, and C. W. Bauschlicher, J. Chem. Phys. **80**, 4378 (1984).

[37] P. S. Bagus, K. Hermann, and C. W. Bauschlicher, J. Chem. Phys. **81**, 1966 (1984).

[38] DACAPO pseudopotential code (https://wiki.fysik.dtu.dk/dacapo), Center for Atomic-scale Materials Design (CAMD), Technical University of Denmark, Lyngby, 2009.

[39] See supplementary material at http://dx.doi.org/10.1063/1.3292681 for Cartesian coordinates of structural models as well as parameters and orbital basis sets for the Pt ECP.

[40] T. A. Wesolowski and A. Warshel, J. Phys. Chem. **97**, 8050 (1993).

[41] M. Levy, Proc. Natl. Acad. Sci. U.S.A. **76**, 6062 (1979).

[42] Sh. Meng, E. G. Wang, and S. Gao, Phys. Rev. B **69**, 195404 (2004).

[43] N. Godbout, D. R. Salahub, J. Andzelm, and E. Wimmer, Can. J. Chem. **70**, 560 (1992). The DZVP2 Cu basis set was taken from the DGauss basis set library.

[44] A. Mattsson, I. Panas, P. Siegbahn, U. Wahlgren, and H. Åkeby, Phys. Rev. B **36**, 7389 (1987).

[45] U. Wahlgren (unpublished), for parameters and orbital basis sets see Ref. 39.

[46] V. Bonifacic and S. Huzinaga, J. Chem. Phys. **60**, 2779 (1974).

[47] L. G. M. Pettersson, U. Wahlgren, and O. Gropen, Chem. Phys. **80**, 7 (1983).

[48] L. G. M. Pettersson and A. Strömberg, Chem. Phys. Lett. **99**, 122 (1983).

[49] M. B. Airola and M. D. Morse, J. Chem. Phys. **116**, 1313 (2002).

[50] K. P. Huber and G. Herzberg, *Constants of Diatomic Molecules* (Van Nostrand Reinhold, New York, 1979).

[51] W. Liu and R. Franke, J. Comput. Chem. **23**, 564 (2002).

[52] W. Kutzelnigg, U. Fleischer, and M. Schindler, *NMR-Basic Principles and Progress* (Springer-Verlag, Heidelberg, 1990).

[53] L. G. M. Pettersson, U. Wahlgren, and O. Gropen, J. Chem. Phys. **86**, 2176 (1987).

[54] S. Huzinaga, J. Chem. Phys. **42**, 1293 (1965).

[55] A. D. Becke, Phys. Rev. A **38**, 3098 (1988).

[56] J. P. Perdew, Phys. Rev. B **34**, 7406 (1986).

[57] K. Bange, T. E. Madey, J. K. Sass, and E. Stuve, Surf. Sci. **183**, 334 (1987).

[58] M. Mehlhorn and K. Morgenstern, Phys. Rev. Lett. **99**, 246101 (2007).

[59] Ph. Wernet, D. Nordlund, U. Bergmann, M. Cavalleri, M. Odelius, H. Ogasawara, L. Å. Näslund, T. K. Hirsch, L. Ojamäe, P. Glatzel, L. G. M. Pettersson, and A. Nilsson, Science **304**, 995 (2004).

[60] D. Nordlund, H. Ogasawara, Ph. Wernet, M. Nyberg, M. Odelius, L. G. M. Pettersson, and A. Nilsson, Chem. Phys. Lett. **395**, 161 (2004).

[61] B. Hammer and J. Nørskov, Surf. Sci. **343**, 211 (1995).

[62] A. Nilsson, L. G. M. Pettersson, B. Hammer, T. Bligaard, C. H. Christensen, and J. K. Nørskov, Catal. Lett. **100**, 111 (2005).

[63] J. Ren and Sh. Meng, J. Am. Chem. Soc. **128**, 9282 (2006).

[64] J. Harris and S. Andersson, Phys. Rev. Lett. **55**, 1583 (1985).

[65] R. Smoluchowski, Phys. Rev. **60**, 661 (1941).

[66] C. J. Fall, N. Binggeli, and A. Baldereschi, Phys. Rev. B **61**, 8489 (2000).

[67] A. Nilsson and L. G. M. Pettersson, in *Chemical Bonding at Surfaces and Interfaces*, edited by A. Nilsson, L. G. M. Pettersson, and J. K. Nørskov (Elsevier, Amsterdam, 2008).

[68] K. Kitaura and K. Morokuma, Int. J. Quantum Chem. **10**, 325 (1976).

[69] S. Shou-heng, S. Chuan, K. Fink, and V. Staemmler, Chem. Phys. **287**, 183 (2003).

[70] A. Michaelides and D. King, Phys. Rev. B **69**, 113404 (2004).

[71] J. Carrasco, A. Michaelides, and M. Scheffler, J. Chem. Phys. **130**, 184707 (2009).